Artificial Electro-Optical Neuron Integrating Hot Electrons in a Mott Insulator

Danylo Babich,[1] Laurent Cario,[1,*] Benoit Corraze,[1] Maciej Lorenc,[2] Julien Tranchant,[1] Roman Bertoni,[2] Marco Cammarata,[2] Hervé Cailleau,[2] and Etienne Janod[1,†]

[1] *Nantes Université, CNRS, Institut des Matériaux de Nantes Jean Rouxel, IMN, F-44000 Nantes, France*
[2] *Univ Rennes, CNRS, IPR (Institut de Physique de Rennes), UMR 6251, F-35000 Rennes, France*

(Received 28 June 2021; accepted 5 January 2022; published 28 January 2022)

Mott insulators are a class of strongly correlated materials with emergent properties important for modern electronics applications, such as artificial neural networks. Under an electric field, these compounds undergo a resistive switching that may be used to build up artificial neurons. However, the mechanism of this resistive switching is still under debate and may depend on the Mott material involved. Some works suggest an electronic avalanche phenomenon, while others propose an electrothermal scenario. As electric pulses produce both Joule heating and hot carriers, disentangling their respective roles requires the use of another external stimulus. Here, an ultrashort light pulse is used to tune the number of photogenerated carriers and the energy provided to the system. In these pump-pump-probe experiments, a crystal of the Mott insulator $GaTa_4Se_8$ is simultaneously excited by electric and laser pulses while an electric probe monitors its conductivity. The study shows that the resistive switching is affected by the number of generated photocarriers rather than by the accumulation of energy deposited by the femtosecond laser. It supports therefore a mechanism driven by generation of hot carriers. Finally, our work opens the possibility to build up an artificial electro-optical "Mott" neuron tuned by a femtosecond laser pulse.

DOI: 10.1103/PhysRevApplied.17.014040

I. INTRODUCTION

Modern artificial intelligence (AI) technology is currently based on the emulation of biological neural networks on classical von Neumann computers [1]. However, the current approach is less efficient than the mammal brain in terms of energy consumption. In that regard, one of the most challenging issues for AI is the implementation of neural network components in hardware [2–5]. The classical biological neural circuit consists of neurons interconnected by synapses that modulate the interneuron signal transfer. The main building block of the brain, i.e., the biological neuron, accumulates incoming signals during the "integration time" and "fires" (generates an output signal) once the integration reaches a threshold. The creation of artificial neurons requires therefore materials possessing a physical property able to implement both integrate and fire functionalities with a clear identification of the physical quantity that is integrated [3,6,7]. One of the possible solutions, currently under investigation, is the use of a class of quantum materials, the Mott insulators [8–10], which exhibit an insulator-to-metal transition (IMT) under an electric field, the so-called electric Mott transition (EMT) [11]. The main signature of this EMT is a resistive switching occurring under the electric field and that has been explained by different mechanisms depending on the investigated Mott materials. For VO_2, the resistive switching is proposed to originate from the self-Joule heating generated during the electric pulse [11–14]. Conversely, in the Mott insulators AM_4Q_8, $(V_{1-x}Cr_x)_2O_3$, and $NiS_{2-x}Se_x$, the resistive switching is associated with the creation of hot carriers followed by an electronic avalanche phenomenon [15–17]. As several recent studies show the impact of light on the Mott transition [18–20], we reinvestigate here the resistive switching mechanism of a $GaTa_4Se_8$ crystal using a pump-pump-probe experiment with simultaneous electric and laser pulse excitation and electrical conductivity probing. Our study shows that photodoping provided by a laser pulse impacts the EMT dynamics. By tuning the number of photogenerated carriers and the energy provided to the system, we shed light on the physical quantity that is integrated in this Mott material [21] and establish the proof-of-concept of an artificial electro-optical "Mott" neuron.

II. EXPERIMENTAL DETAILS

A. Sample preparation and characterization

$GaTa_4Se_8$ crystals are synthesized by a method described elsewhere [34], and cleaved into 200–300 μm pieces. Crystals used for transport measurements are contacted using 10-μm gold wires and carbon paste (Electrodag PR-406), and then annealed under vacuum at 150 °C for 30 min. The low-bias resistance is measured using

*laurent.cario@cnrs-imn.fr
†etienne.janod@cnrs-imn.fr

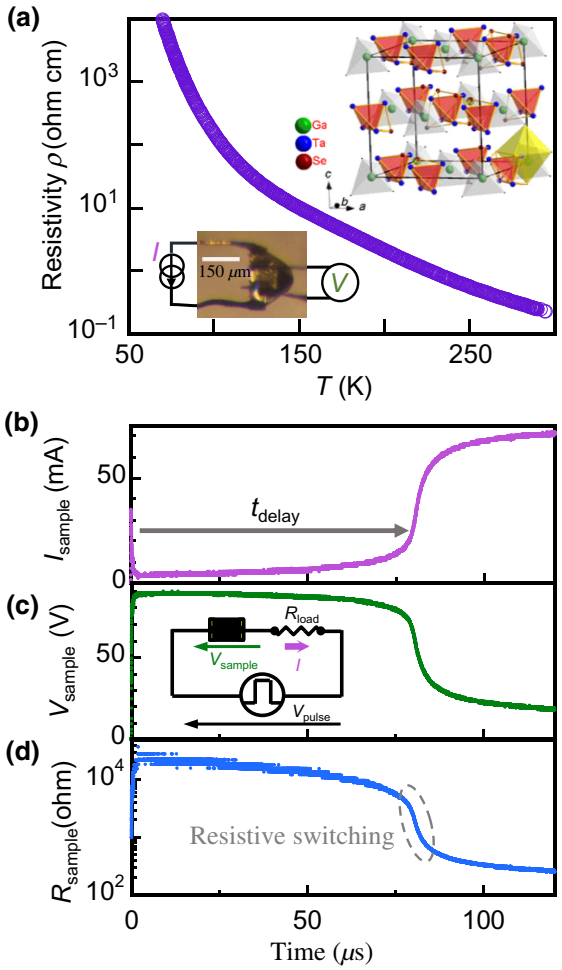

FIG. 1. (a) Resistivity versus temperature measured on a single crystal of the Mott insulator $GaTa_4Se_8$. The insets show the crystallographic structure of $GaTa_4Se_8$ and a picture of the $GaTa_4Se_8$ single crystal connected with four gold wires. (b)–(d) A typical example of an electric Mott transition induced at 85 K by the application of a 120-μs (90-V) electric pulse on a circuit made of the $GaTa_4Se_8$ crystal in series with a 1-kΩ load resistance. The temporal evolutions of the current (b), of the sample voltage (c), and of the sample resistance (d) clearly indicate a resistive switching occurring after a time delay of approximately 80 μs.

a Keithley 236 source-measure unit by a standard two- or four-probe technique [Fig. 1(a)]. For the application of electric pulses, we connect two gold wires along the crystal surface on which light should be applied. The inter-electrode distance is around 200 μm.

B. Pump-pump-probe experiments

We apply two "pumps," an approximately 100-μs electric pulse and a 100-fs laser pulse in a single-shot mode, on the $GaTa_4Se_8$ crystal, as we record the evolution of the electric resistance ("probe"). We use a Ti:sapphire femtosecond laser synchronized with an electric pulse generator (Keithley 8114A) so that the laser output is triggered precisely with the first nanoseconds of the electrical pulse. During the pulse, the voltage and current across the sample are measured with a Tektronix DPO3034 oscilloscope associated with IeS-ISSD210 differential probes. We use an optical parametric amplifier (OPA) to tune the laser wavelength from the visible to mid-IR region. In order to control the crystal temperature, we use a nitrogen cryostream. We carry out the experiments with the same number of absorbed photons by taking care to keep the laser spot size similar at the different wavelengths. We use a short-focus (5 cm) optical lens. After the experiment with the $GaTa_4Se_8$ single crystal, we perform knife-edge measurements to recover the spatial profile of the laser beam. It allows a reliable estimate of the beam size, which are similar for both laser energies (0.5 and 2.3 eV) and cover more than 90% of the inter-electrode area. In these experiments, the level of photodoping depends on both the laser fluence and the impacted volume. The latter is defined by the size of the beam hitting the sample surface and a characteristic length over which the photocarriers spread inside the materials. Since photodoped carriers are subjected to applied dc electric fields E close to 3 kV/cm, this characteristic length corresponds to the diffusion length of the carriers rather than the initial absorption length (i.e., the light penetration depth). The diffusion length is indeed defined as $l_{\mathrm{diff}} = \mu E \tau$, where μ and τ are the carrier mobility and lifetime, respectively. Considering a lifetime of 1 μs typical of AM_4Q_8 compounds [35] and a mobility representative of Mott insulators of 1 $\mathrm{cm}^2/(\mathrm{Vs})$ [36] leads to a lower limit of 30 μm for the diffusion length. This value exceeds the typical light penetration depth by more than 2 orders of magnitude. Consequently, experiments conducted with similar beam sizes and density of absorbed photons, but with laser pulses at different wavelengths, will yield analogous levels of photodoping.

III. RESULTS AND DISCUSSION

According to conventional band theory, Mott insulators should be metallic. Their insulating ground state results from the on-site electron-electron Coulombic repulsion, not accounted for in the classical approach, which favors the localization of electrons on atomic sites. At equilibrium, the insulating state can be broken by pressure or charge doping. Recently, an insulator-to-metal transition leading to a resistive switching was also achieved under an electric field in Mott insulators [11,15,22,23]. This phenomenon, also called EMT, was observed for numerous examples of Mott insulators. In this paper, we focus on a member of the family of narrow gap chalcogenide Mott insulators of formulation AM_4Q_8 (A = Ga, Ge; M = V, Nb, Ta, Mo; Q = S, Se) that exhibit a clustered lacunar spinel structure [24–27]. Figure 1 presents the thermal

dependence of the resistivity and a typical resistive switching phenomenon observed in a crystal of $GaTa_4Se_8$. For this compound, the proposed microscopic mechanism for resistive switching is based on Fröhlich's theory of dielectric breakdown [28,29]. The details of this theory and its application to the AM_4Q_8 Mott insulators are published elsewhere [16]. The model considers the existence of small numbers of electrons either trapped in localized levels below the conduction band or delocalized in the conduction band. These latter pre-existing free carriers can be accelerated under an electric field and share their energy with other electrons and the lattice thanks to, respectively, electron-electron (e-e) or electron-phonon (e-ph) interactions [16]. New hot carriers are generated under an electric field, which increases the overall electronic temperature until a new equilibrium situation is reached between the power given to (electric power) and the power taken out from (e-ph) the electronic system (i.e., it corresponds to a two-temperature model with the electronic temperature stabilizing slightly over that of the lattice). But once the applied electric field reaches a threshold value E_{th}, the equilibrium between the lattice and electronic subsystems cannot be maintained, and the system enters into a nonequilibrium state with the number of hot carriers diverging and inducing an IMT (i.e., the resistive switching). The theory predicts a temperature-independent deviation from Ohm's law below the threshold field ($E \ll E_{\text{th}}$) with the multiplication rate of new carriers in the conduction band $\tilde{n} = n/n_0$ depending only on the square of the electric field if we assume the mobility to be constant:

$$\tilde{n} = \frac{n}{n_0} = \frac{\sigma(E)}{\sigma_0} = exp\left(\frac{E^2 \varepsilon_G}{E_{\text{th}}^2 e \Delta\varepsilon}\right), \tag{1}$$

where n_0 and σ_0 are the number of carriers and conductivity at zero field. Constants ε_G and $\Delta\varepsilon$ represent the width of the gap and of the in-gap state levels, respectively, and e is Euler's constant. In the boundary case of the prediction ($E = E_{\text{th}}$), the threshold value of the carrier multiplication rate $\tilde{n}_{\text{th}}$ becomes

$$\tilde{n}_{\text{th}} = exp\left(\frac{\varepsilon_G}{\Delta\varepsilon}\right). \tag{2}$$

In our previous work, the low-field conductivity of the narrow-gap Mott insulators AM_4Q_8 was compared with these predictions using the experimental values for the gap ε_G and for $\Delta\varepsilon$ (e.g., $\varepsilon_G = 158$ meV and $\Delta\varepsilon = 112$ meV in the case of $GaTa_4Se_8$) [16]. As displayed in Fig. 2(a), the measurements, performed at different temperatures for a $GaTa_4Se_8$ crystal, lie on the predictable master curve for the carrier multiplication rate $\tilde{n}$ (see blue line). It fully supports the proposed model suggesting that, below the threshold field, $\tilde{n}$ may stabilize in time, while above the threshold electric field (when the system exceeds the

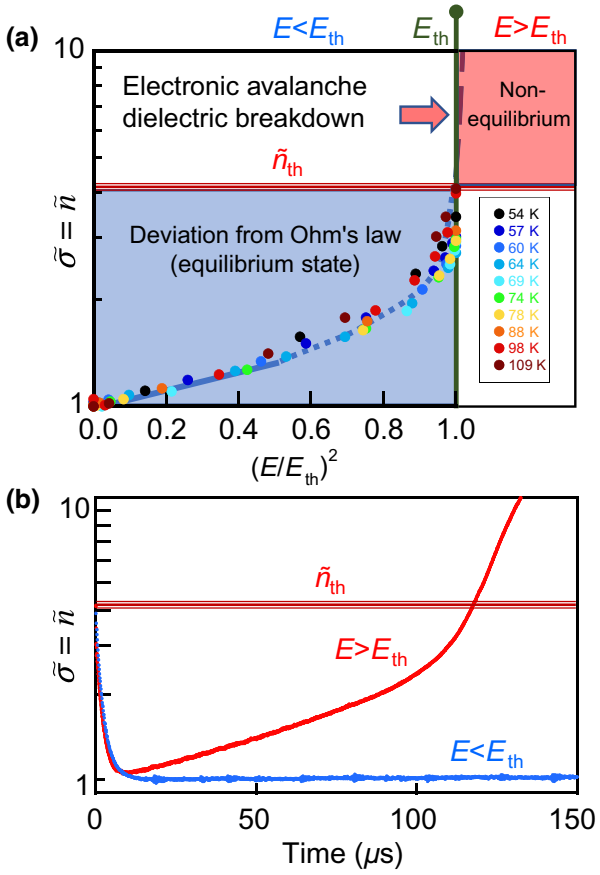

FIG. 2. (a) Transport measurements performed at different temperatures and low electric field for a $GaTa_4Se_8$ crystal. All measurements fall on a master curve following the predicted evolution of the carrier multiplication rate $\tilde{n}$ (blue dotted line). (b) Conductivity ratio dynamics $\tilde{\sigma} = \sigma/\sigma_0$ measured under electric field for a $GaTa_4Se_8$ crystal for $E < E_{\text{th}}$ and $E > E_{\text{th}}$.

threshold carrier multiplication rate $\tilde{n}_{th}$ slightly greater than 4 in our experiments) $\tilde{n}$ can no longer stabilize and may diverge in time. Figure 2(b) presents the experimental conductivity ratio dynamics $\tilde{\sigma} = \sigma/\sigma_0$ measured under an electric field for a $GaTa_4Se_8$ crystal. Below E_{th} (ranging from 0.3 to 7 kV/cm in $GaTa_4Se_8$ depending on the temperature [16]), the conductivity ratio stabilizes over time and the system remains insulating, which means the electronic temperature reaches an equilibrium. But for electric field higher than the threshold value ($E > E_{\text{th}}$) a sudden increase of the conductivity ratio appears (i.e., a volatile resistive switching occurs) as the carrier multiplication rate approaches $\tilde{n}_{\text{th}}$ and the system enters into an avalanche carrier multiplication regime [Fig. 2(a)].

According to the model, new hot carriers are accumulated in the AM_4Q_8 compounds under the electric field. This model is therefore of great interest in the framework of neurocomputing as it suggests that the AM_4Q_8 compounds behave as hot carrier integrators. Similar to

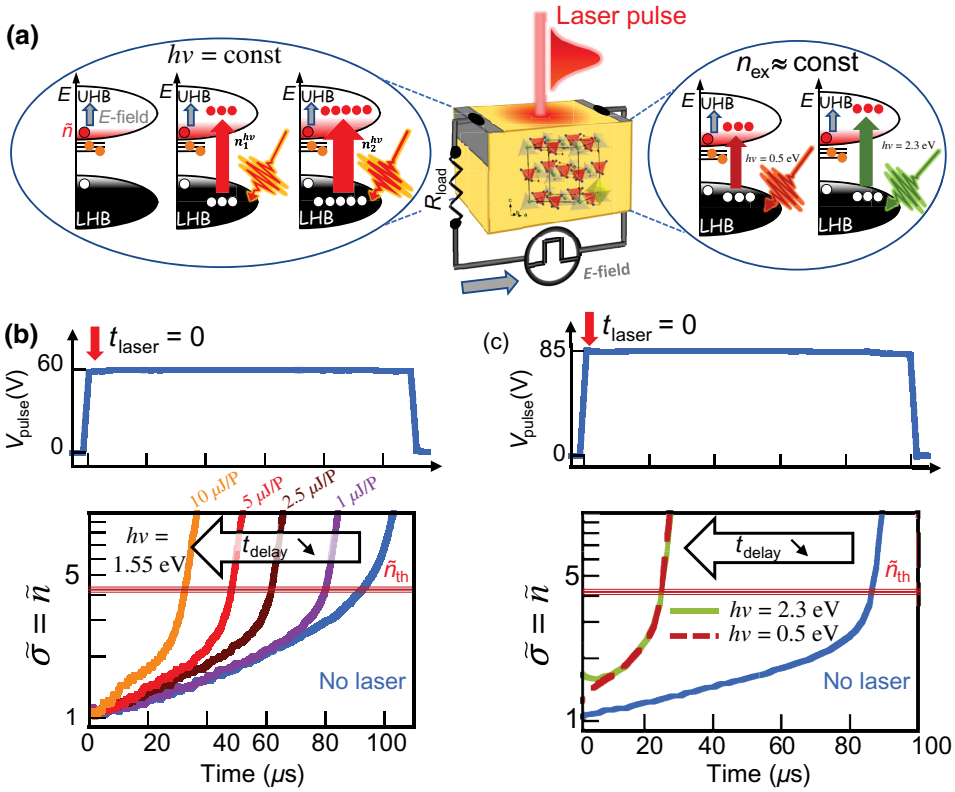

FIG. 3. Temporal evolution of the normalized conductivity $\tilde{\sigma} = \sigma/\sigma_0$ during a voltage pulse applied to different circuits containing a $GaTa_4Se_8$ crystal and that is synchronized or not with a single-shot 100-fs laser pulse applied at the beginning of the pulse. (a) Schematic representation of the setup and impact of laser fluence or wavelength on the number of electrons excited from the lower (LHB) to the upper Hubbard band (UHB). (b) Evolution of $\tilde{\sigma}(t)$ measured under a 60-V voltage pulse and when femtosecond laser pulses of constant energy (800 nm, $h\nu = 1.55$ eV) and of increasing fluences are applied (from 1 to 10 μJ/pulse). (c) Evolution of $\tilde{\sigma}(t)$ measured on a different $GaTa_4Se_8$ crystal under an 85-V voltage pulse and when femtosecond laser pulses leading to the same number of induced photocarriers are applied with two different energies ($h\nu = 0.5$ and 2.3 eV).

biological neurons that accumulate charges on their membranes until the membrane potential reaches a threshold, the Mott insulators accumulate hot carriers until the carrier multiplication rate reaches a threshold. In order to support this scenario, we compare the carrier multiplication rate dynamics obtained under an electric pulse alone or when the electric pulse is coupled to a laser pulse in order to modify the carrier number. The setup sketched in Fig. 3 is used to implement this electro-optical pump and electric probe experiment. A freshly cleaved surface of a $GaTa_4Se_8$ single crystal is connected by two gold electrodes separated by about 200 μm to allow the use of ultrashort laser pulses with a fixed spot size slightly smaller than the inter-electrodes distance. We use a femtosecond Ti:sapphire regenerative amplifier and an OPA to tune the wavelength of the optical pump between visible and infrared. The electrodes are used both to apply the electric field via a pulse generator and to monitor conductivity dynamics via an oscilloscope connected in parallel. The setup works in single-shot mode with a synchronous application of the electric and laser pulses. We perform all experiments under nitrogen cryostream cooling at 85 ($\pm$5) K in order to have optimal stability conditions to induce the resistive switching experiments.

In a first series of experiments, we simultaneously apply electrical voltage pulses of 60 V (i.e., exceeding the threshold value) and 800-nm ($h\nu = 1.55$ eV) femtosecond pulses, while varying the excitation density. As depicted in Fig. 3(a), the main idea is to tune the number of photoexcited carriers at the beginning of the electric pulse. Figure 3(a) shows that the concomitant application of an optical excitation drastically reduces the time delay necessary to observe the resistive switching. Moreover, this time delay decreases when the excitation density increases. These experiments already evidence a clear impact of photoexcited carriers on the resistive switching. They suggest a similar role of hot carriers generated by light or electric field. This result supports that the photoexcited carriers are added to the hot electrons accumulated under the electric field to reach the threshold carrier multiplication rate and promote the avalanche phenomenon. A possible impact of the thermal energy injected into the system (lattice and

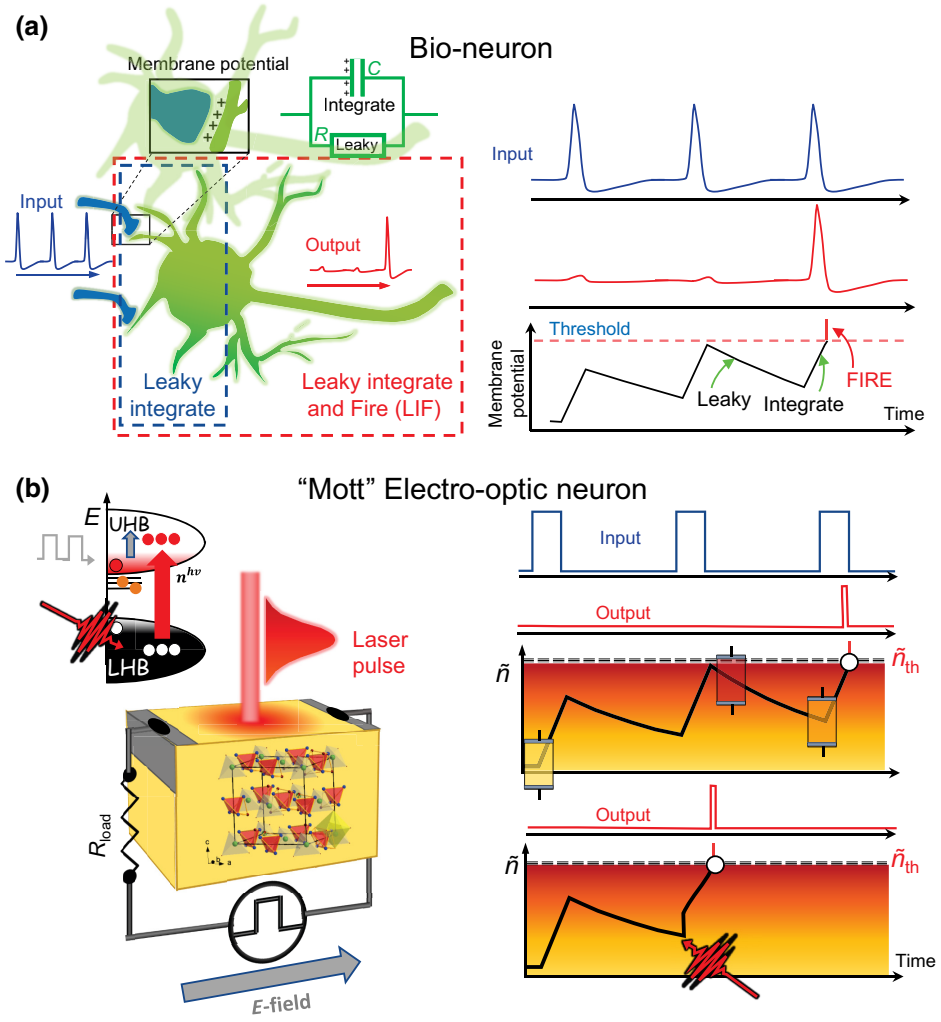

FIG. 4. (a) Schematic of a biological neuron receiving input spikes from other neurons and triggering an output action potential when the membrane potential reaches a threshold value. This behavior of the neuron membrane was first modeled by a *RC* circuit and led to the definition of the simplest model of artificial neuron called LIF. (b) Sketch of an electro-optic Mott neuron setup and graphical representation of the electronic dynamics with or without laser pulse. The artificial Mott neuron follows dynamics similar to that of the LIF model but the integrated quantity is not the membrane potential (or the charge in the capacitor) but the carrier multiplication rate ($\tilde{n}$) in the Mott device.

electrons) by the light pulse cannot be completely discarded based on this experiment alone as at the probed time scale both subsystems should have reached thermal distributions (Fermi-Dirac and Bose-Einstein).

Another way to address this issue is to tune the excitation density and the photon energy of the pulse using the OPA. As sketched in Fig. 3(b), the main objective of these experiments is to tune the photon energy while keeping a constant number of photons. This series of experiments are conducted using another $GaTa_4Se_8$ crystal in a configuration similar to that depicted in Fig. 3(a). The boundary values of the photon energies used ($h\nu$) are 0.5 and 2.3 eV. The fluence is set to 2.5 μJ/pulse for $h\nu = 0.5$ eV and to 8.8 μJ/pulse for $h\nu = 2.3$ eV. These values correspond to 7×10^{16} and 5.5×10^{16} absorbed photons per cm^2, respectively, and hence to almost similar densities of photodoped carriers (see discussion in Sec. II). Electrical measurements presented in Fig. 3(b) demonstrate no change in carrier multiplication rate dynamics under electric field independently of the used photon energies (0.5 and 2.3 eV, respectively). In particular, the time delays required to reach $\tilde{n}_{th}$ (i.e., the resistive switching) are remarkably similar while the energy provided by the light pulses changes by a factor of approximately 3.5 (8.8 μJ against 2.5 μJ). It demonstrates that the key parameter of the optical excitation that controls the resistive switching *is not* a trivial photothermal effect in agreement with a recent study on the V_2O_3 antiferromagnetic Mott insulating phase [30]. Conversely, it suggests that the relevant parameter driving the electric Mott transition in $GaTa_4Se_8$ is rather the number of hot carriers generated. Mott insulators appear therefore as hot carrier integrators that undergo a resistive switching when the carrier multiplication rate ($\tilde{n}$) reaches a threshold value depending only on intrinsic material features and/or properties.

All these findings are of great interest to build up an electro-optical Mott neuron for artificial neuromorphic devices [3,5] and neuromorphic photonics [31,32]. As depicted in Fig. 4(a), when a biological neuron receives input spikes from other neurons, they are integrated into the membrane potential. In between the incoming spikes, the membrane potential relaxes, which is known as a leaky behavior. Finally, when the membrane potential reaches a threshold value, the neuron triggers an output action

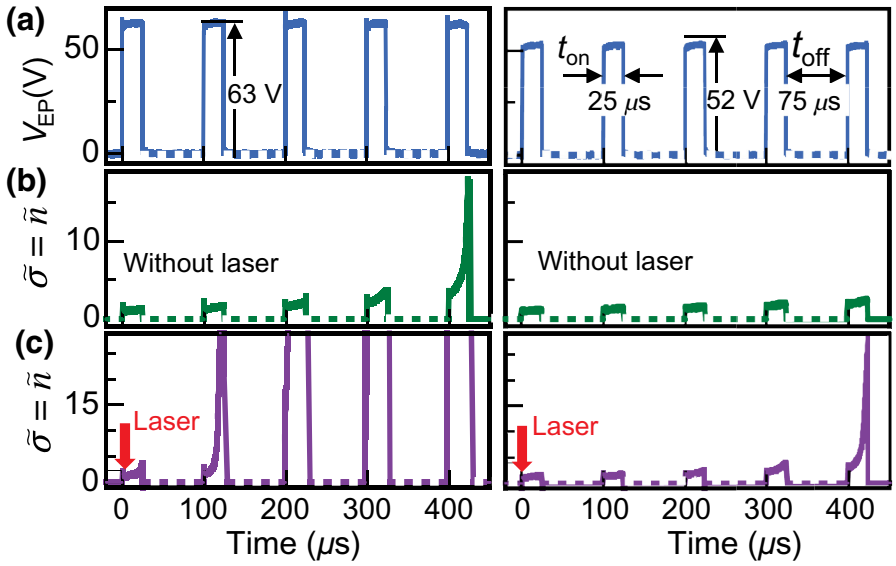

FIG. 5. Experimental resistive switching obtained by applying trains of 25-μs electric pulses of 63 or 52 V synchronized or not with a 100-fs laser pulse. (a) Profile of applied voltage pulses. Sample conductivity time profiles measured (b) without and (c) with laser pulse. The measurements are performed under conditions similar to the ones of Fig. 3(a).

potential (firing event). The biological neuron implements, therefore, three important functionalities that are at the basis of the most used model of an artificial neuron, namely the leaky, integrate, and fire (LIF) artificial neuron. In a previous work, we have demonstrated that the AM_4Q_8 compounds, as well as other Mott insulators like $(V_{1-x}Cr_x)_2O_3$ or [Au(iPr-thiazdt)$_2$], behave as LIF artificial neurons [9]. This behavior is observed when a crystal of Mott insulator is subjected to a train of electrical pulses. Figures 5(a)–5(c) show the results of other experiments intended to control the Mott neuron also by light, and for which an ultrashort laser pulse is synchronized with the first electrical pulse of the train. These experiments are conducted by applying the train of electrical pulses and laser pulses on a $GaTa_4Se_8$ crystal using a setup similar to that shown in Fig. 4(b). The green curves in Fig. 5(b) represent conductivity ratio or carrier multiplication rate measured without a laser. When electric pulses of 63 V are applied, the system fires (i.e., a resistive switching is observed) during the fifth pulse while no firing event is observed when pulses of 52 V are used. Applying a laser pulse (10 μJ/pulse, $h\nu = 1.55$ eV) at the beginning of the train of electric pulses has a strong impact on the behavior of the Mott neuron. Indeed, the firing event occurs much sooner compared with the case without optical excitation. For electrical pulses of 63 V, it occurs after only two electrical pulses while it appears in the fifth pulse when using 52 V (see violet curves). There is a striking difference as no firing event is recorded with electrical stimulus only. These experiments demonstrate a clear impact of an ultrashort light pulse on the behavior of the Mott artificial neuron. They reveal that ultrashort light pulses could be used as a new external parameter to tune the firing time of the device. At this step the device is made with a single crystal and for this reason the LIF behavior is observed at low temperature using quite high voltage pulses. But our previous works on artificial Mott neurons have already demonstrated that the working conditions can be much improved by using thin-film devices [9,33]. Indeed the downscaling of a thin-film device allows one to lower the operational voltage to a few volts and to increase the working temperature towards room temperature. The experiments reported in this paper and performed on single crystals open, therefore, the door to the realization of artificial electro-optical Mott neurons made of thin films that would be promising components for neuromorphic photonics [31,32].

IV. CONCLUSIONS

To conclude, the electro-optical pump-electrical probe measurements presented in this work demonstrate the possibility to control the dynamics of the electric Mott transition by ultrashort laser pulses in the Mott insulator $GaTa_4Se_8$. They further confirm that light and an electric field can act synergistically to induce an insulator-to-metal transition in a Mott insulator. These results are compatible with an electric Mott transition mechanism based on a carrier multiplication phenomenon whose dynamics can be modified as a result of the generation of extra photocarriers by optical excitation. The obtained results demonstrate that Mott insulators behave under an electric field as leaky integrators of hot carriers, more precisely of carrier multiplication rate. When the carrier multiplication rate reaches a threshold value, the firing event (i.e., resistive switching) occurs. Hot carriers and carrier multiplication rates are, therefore, the physical quantities of interest to control a Mott neuron. Beyond this fundamental output, we also show that both light and electric field stimuli can control the dynamics of the Mott artificial neuron. Our work demonstrates an interesting concept of the electro-optical

artificial Mott neuron and opens an alternative path in the emerging field of neuromorphic photonics [31,32].

ACKNOWLEDGMENTS

All authors gratefully acknowledge Agence Nationale de la Recherche for financial support under Grant No. ANR-16-CE30-0018 ("Elastica"). D.B. thanks University of Nantes for financial support in the framework of the IM-LED LIA (CNRS).

[1] A. K. Jain, J. Mao, and K. M. Mohiuddin, Artificial neural networks: A tutorial, Computer **29**, 31 (1996).
[2] J. Misra and I. Saha, Artificial neural networks in hardware: A survey of Two decades of progress, Neurocomputing **74**, 239 (2010).
[3] G. Indiveri and T. K. Horiuchi, Frontiers in neuromorphic engineering, Front. Neurosci. **5**, 118 (2011).
[4] D. Seok Jeong, I. Kim, M. Ziegler, and H. Kohlstedt, Towards artificial neurons and synapses: A materials point of view, RSC Adv. **3**, 3169 (2013).
[5] J. Zhu, T. Zhang, Y. Yang, and R. Huang, A comprehensive review on emerging artificial neuromorphic devices, Appl. Phys. Rev. **7**, 011312 (2020).
[6] A. N. Burkitt, A review of the integrate-and-fire neuron model: I. homogeneous synaptic input, Biol. Cybern. **95**, 1 (2006).
[7] A Review of the Integrate-and-Fire Neuron Model: I. Homogeneous Synaptic Input. - ResearchGate (2006).
[8] P. Stoliar, J. Tranchant, B. Corraze, E. Janod, M.-P. Besland, F. Tesler, M. Rozenberg, and L. Cario, A leaky-integrate-and-fire neuron analog realized with a Mott insulator, Adv. Funct. Mater. **27**, 1604740 (2017).
[9] C. Adda, B. Corraze, P. Stoliar, P. Diener, J. Tranchant, A. Filatre-Furcate, M. Fourmigué, D. Lorcy, M.-P. Besland, E. Janod, and L. Cario, Mott insulators: A large class of materials for leaky integrate and fire (LIF) artificial neuron, J Appl. Phys. **124**, 152124 (2018).
[10] F. Tesler, C. Adda, J. Tranchant, B. Corraze, E. Janod, L. Cario, P. Stoliar, and M. Rozenberg, Relaxation of a Spiking Mott Artificial Neuron, Phys. Rev. Appl. **10**, 054001 (2018).
[11] E. Janod, J. Tranchant, B. Corraze, M. Querré, P. Stoliar, M. Rozenberg, T. Cren, D. Roditchev, V. T. Phuoc, M.-P. Besland, and L. Cario, Resistive switching in Mott insulators and correlated systems, Adv. Funct. Mater. **25**, 6287 (2015).
[12] B. S. Mun, J. Yoon, S.-K. Mo, K. Chen, N. Tamura, C. Dejoie, M. Kunz, Z. Liu, C. Park, K. Moon, and H. Ju, Role of joule heating effect and bulk-surface phases in voltage-driven metal-insulator transition in VO_2 crystal, Appl. Phys. Lett. **103**, 061902 (2013).
[13] S. Kumar, M. D. Pickett, J. P. Strachan, G. Gibson, Y. Nishi, and R. S. Williams, Local temperature redistribution and structural transition during joule-heating-driven conductance switching in VO_2, Adv. Mater. **25**, 6128 (2013).
[14] A. Zimmers, L. Aigouy, M. Mortier, A. Sharoni, S. Wang, K. G. West, J. G. Ramirez, and I. K. Schuller, Role of Thermal Heating on the Voltage Induced Insulator-Metal Transition in VO_2, Phys. Rev. Lett. **110**, 056601 (2013).
[15] V. Guiot, L. Cario, E. Janod, B. Corraze, V. Ta Phuoc, M. Rozenberg, P. Stoliar, T. Cren, and D. Roditchev, Avalanche breakdown in $GaTa_4Se_{8-x}Te_x$ narrow-Gap Mott insulators, Nat. Commun. **4**, 1722 (2013).
[16] P. Diener, E. Janod, B. Corraze, M. Querré, C. Adda, M. Guilloux-Viry, S. Cordier, A. Camjayi, M. Rozenberg, M. P. Besland, and L. Cario, How a Dc Electric Field Drives Mott Insulators Out of Equilibrium, Phys. Rev. Lett. **121**, 016601 (2018).
[17] P. Stoliar, L. Cario, E. Janod, B. Corraze, C. Guillot-Deudon, S. Salmon-Bourmand, V. Guiot, J. Tranchant, and M. Rozenberg, Universal electric-field-driven resistive transition in narrow-Gap Mott insulators, Adv. Mater. **25**, 3222 (2013).
[18] E. Abreu, D. Babich, E. Janod, S. Houver, B. Corraze, L. Cario, and S. Johnson, in *2019 44th International Conference on Infrared, Millimeter, and Terahertz Waves (IRMMW-THz)* (IEEE, Paris, France, 2019), pp. 1–2.
[19] H. Yamakawa, T. Miyamoto, T. Morimoto, T. Terashige, H. Yada, N. Kida, M. Suda, H. M. Yamamoto, R. Kato, K. Miyagawa, K. Kanoda, and H. Okamoto, Mott transition by an impulsive dielectric breakdown, Nat. Mater. **16**, 1100 (2017).
[20] F. Giorgianni, J. Sakai, and S. Lupi, Overcoming the thermal regime for the electric-field driven Mott transition in vanadium sesquioxide, Nat. Commun. **10**, 1 (2019).
[21] J. Tranchant, E. Janod, B. Corraze, P. Stoliar, M. Rozenberg, M.-P. Besland, and L. Cario, Control of resistive switching in AM_4Q_8 narrow Gap Mott insulators: A first step towards neuromorphic applications, Phys. Status Solidi A **212**, 239 (2015).
[22] Y. Taguchi, T. Matsumoto, and Y. Tokura, Dielectric breakdown of One-dimensional Mott insulators Sr_2CuO_3 and $SrCuO_2$, Phys. Rev. B **62**, 7015 (2000).
[23] G. Stefanovich, A. Pergament, and D. Stefanovich, Electrical switching and Mott transition in VO_2, J. Phys.: Condens. Matter **12**, 8837 (2000).
[24] H. B. Yaich, J. C. Jegaden, M. Potel, R. Chevrel, M. Sergent, A. Berton, J. Chaussy, A. K. Rastogi, and R. Tournier, Nouveaux chalcogenures mixtes $GaMo_4(XX')_8$ (X = S, Se, Te) à clusters tetraedriques Mo_4, J. Solid State Chem. **51**, 212 (1984).
[25] R. Pocha, D. Johrendt, B. Ni, M. M. Abd-Elmeguid, Crystal Structures, and Electronic Properties, And pressure-induced superconductivity of the tetrahedral cluster compounds $GaNb_4S_8$, $GaNb_4Se_8$, and $GaTa_4Se_8$, J. Am. Chem. Soc. **127**, 8732 (2005).
[26] D. Bichler, V. Zinth, D. Johrendt, O. Heyer, M. K. Forthaus, T. Lorenz, and M. M. Abd-Elmeguid, Structural and magnetic phase transitions of the V_4-cluster compound GeV_4S_8, Phys. Rev. B **77**, 212102 (2008).
[27] V. Guiot, E. Janod, B. Corraze, and L. Cario, Control of the electronic properties and resistive switching in the New series of Mott insulators $GaTa_4Se_8 - yTey$ $(0 \leq y \leq 6.5)$, Chem. Mater. **23**, 2611 (2011).
[28] H. Fröhlich and N. F. Mott, Theory of electrical breakdown in ionic crystals, Proc. R. Soc. London, Ser. A **160**, 230 (1937).

[29] H. Fröhlich and N. F. Mott, On the theory of dielectric breakdown in solids, Proc. R. Soc. London, Ser. A **188**, 521 (1947).

[30] A. Ronchi, P. Franceschini, P. Homm, M. Gandolfi, G. Ferrini, S. Pagliara, F. Banfi, M. Menghini, J. P. Locquet, and C. Giannetti, Light-Assisted Resistance Collapse in a V_2O_3-Based Mott-Insulator Device, Phys. Rev. Appl. **15**, 044023 (2021).

[31] E. Goi, Q. Zhang, X. Chen, H. Luan, and M. Gu, Perspective on photonic memristive neuromorphic computing, PhotoniX **1**, 3 (2020).

[32] P. R. Prucnal, B. J. Shastri, and M. C. Teich, *Neuromorphic Photonics* (CRC Press, 2017), 1st ed.

[33] C. Adda, L. Cario, J. Tranchant, E. Janod, M.-P. Besland, M. Rozenberg, P. Stoliar, and B. Corraze, First demonstration of "leaky integrate and fire" artificial neuron behavior on $(V_{0.95}Cr_{0.05})_2O_3$ thin film, MRS Commun. **8**, 835 (2018).

[34] C. Vaju, L. Cario, B. Corraze, E. Janod, V. Dubost, T. Cren, D. Roditchev, D. Braithwaite, and O. Chauvet, Electric-Pulse-Driven electronic phase separation, insulator–metal transition, and possible superconductivity in a Mott insulator, Adv. Mater. **20**, 2760 (2008).

[35] D. Babich, K. Fukumoto, B. Corraze, J. Tranchant, M. Lorenc, H. Cailleau, S.-Y. Koshihara, L. Cario, and E. Janod, in *Frontiers in Optics + Laser Science APS/DLS (2020), Paper LTu8F.3* (Optical Society of America, 2020), pp. LTu8F.3.

[36] J. C. Petersen, A. Farahani, D. G. Sahota, R. Liang, and J. S. Dodge, Transient terahertz photoconductivity of insulating cuprates, Phys. Rev. B **96**, 115133 (2017).